Supplementary Data

1. Supplementary Materials and Methods

In-house compound library

The boronic acid-based proteasome inhibitor library was developed by Dr. Runtao Li's research group, which has optimized these inhibitors over multiple iterations (CN106146542A, CN108368133A, CN114075227A).

Giemsa staining

Peripheral blood smears were prepared from *Pb*-infected mice and stained with Giemsa (Solarbio, G1010). Stained slides were rinsed, air-dried, and mounted for microscopic examination to determine the percentage of iRBCs.

Pharmacokinetic Study

The pharmacokinetic study of Glutoborin in Sprague-Dawley (SD) rats was conducted by Beijing Yingkerui Drug Safety and Efficacy Research Co., Ltd.

Methods of the synthesis of Glutoborin

All reagents and solvents were purchased from commercial suppliers and were used without further purification. ^{1}H NMR and ^{13}C NMR spectra were recorded on Bruker AVANCEIII 400 MHz and 100 MHz spectrometer, respectively. High resolution mass spectrum (HRMS) was recorded on a Thermo Scientific Orbitrap Elite MS.

Synthesis of G2

G1 (322 mg, 1 mmol), commercially available, was dissolved in a mixture of acetone (20 ml) and *N, N*-dimethylformamide (5 ml), followed by the addition of potassium carbonate (276 mg, 2 mmol) and 2-chloroethyl p-toluenesulfonate (480 mg, 2 mmol). The reaction mixture was heated to 80 °C for 12 hrs, then cooled to room temperature and concentrated under reduced pressure. The residue was dissolved in ethyl acetate (30 ml), washed with brine, and dried over anhydrous Na_2SO_4. Purification by column

chromatography (silica gel, 25% ethyl acetate in petroleum ether) yielded intermediate G2 as a white solid (345 mg, 90%). ^{1}H NMR (400 MHz, DMSO-d_6) δ 7.59-7.45 (m, 7H), 7.39 (t, J = 7.9 Hz, 1H), 7.04 (s, 1H), 6.97 (ddd, J = 8.2, 2.6, 1.0 Hz, 1H), 5.12 (s, 2H), 4.39-4.32 (m, 2H), 4.13 (q, J = 7.1 Hz, 2H), 4.04-3.97 (m, 2H), 1.16 (t, J = 7.1 Hz, 3H).

Synthesis of G3

G2 (384 mg, 1 mmol) was dissolved in acetone (40 ml), and sodium iodide (300 mg, 2 mmol) was added. The mixture was heated to 80°C for 24 hrs. Separately, *N*-phenylpiperazine (296 mg, 2 mmol) was dissolved in *N, N*-dimethylformamide (10ml) and added to the reaction mixture. The reaction was maintained at 80°C for 12 hrs, then cooled to room temperature and concentrated under reduced pressure. The residue was dissolved in ethyl acetate (30 ml), washed with brine, and dried over anhydrous Na_2SO_4. Purification by column chromatography (silica gel, 33% ethyl acetate in petroleum ether) afforded G3 as a light-yellow oil (375 mg, 67%). ^{1}H NMR (400 MHz, $CDCl_3$) δ 7.50-7.39 (m, 7H), 7.34-7.23 (m, 3H), 6.96-6.81 (m, 4H), 6.63 (s, 1H), 4.89 (s, 2H), 4.19 (dt, J = 14.2, 4.4 Hz, 4H), 3.27-3.13 (m, 4H), 2.87 (t, J = 5.7 Hz, 2H), 2.76-2.68 (m, 4H), 1.21 (t, J = 7.1 Hz, 3H).

Synthesis of G4

G3 (510 mg, 1 mmol) was suspended in distilled water (15 ml), and 4N HCl (2 ml) was added. The mixture was refluxed overnight, and the water was removed under reduced pressure to afford G4 as grey foam solid (463mg, 96% yield), under directly without further purification.

Synthesis of G5

G4 (482 mg, 1 mmol) was dissolved in *N, N*-dimethylformamide (25 ml), followed by the addition of O-Benzotriazole-*N,N,N′,N′*-tetramethyl-uronium-hexaf (HBTU) (379 mg, 1 mmol). After stirring for 30 min, (*R*)-3-methyl-1-(4,4,5,5-tetramethyl-1,3,2-

dioxaborolan-2-yl)butan-1-amine hydrochloride (298 mg, 1.2 mmol) and *N, N*-diisopropyl diethylamine (DIPEA) (154 mg, 1.2 mmol) were added, and the reaction continued overnight. The reaction was quenched with water, the mixture was extracted with ethyl acetate (30 ml), washed with brine, dried over anhydrous Na_2SO_4, and concentrated under reduced pressure to afford G5 as grey solid (433 mg, 64%), used directly without further purification.

Synthesis of G6

G5 (677 mg, 1 mmol) was dissolved in a mixed solvent of ether (15 ml) and ethyl acetate (3 ml). Diethanolamine (105 mg, 1 mmol) was dissolved in diethyl ether (1 ml) and added dropwise. The reaction mixture was stirred overnight at room temperature, yielding a white precipitate. The solid was filtered, washed with ether, and dried to give G6 as a while solid (398 mg, 60%), used directly without further purification.

Synthesis of Glutoborin

G6 (663 mg, 1 mmol) was suspended in ethyl acetate (20 ml), and distilled water (20 ml) and 4N HCl (2 ml) were added. The reaction mixture was stirred vigorously for 30 min, then basified with saturated $NaHCO_3$ aqueous solution to pH at 8-9. The aqueous phase was extracted with ethyl acetate (3× 20 ml), and the organic layers were combined, washed with water and brine, dried over anhydrous Na_2SO_4, and concentrated under reduced pressure. The resulting solid was recrystallized from ethyl acetate/n-hexane. The purified product was dissolved in ethyl acetate (15 ml), and 2N HCl in ethyl acetate (2 ml) was added. The mixture was stirred overnight at room temperature, affording Glutoborin as a grey solid (601 mg, 90% yield). ^{1}H NMR (400 MHz, DMSO-d_6) δ 7.57-7.55 (m, 2H), 7.50-7.45 (m, 3H), 7.41-7.37 (m, 2H), 7.32 (t, *J* = 7.8 Hz, 1H), 7.21-7.17 (m, 2H), 6.90 -6.87 (m, 4H), 6.76 (t, *J* = 7.2 Hz, 1H), 4.76 (s, 2H), 4.01 (t, *J* = 6.4 Hz, 2H), 3.17-3.13 (m, 1H), 3.09 (t, *J* = 4.6 Hz, 3H), 2.33 (t, *J* = 7.0 Hz, 2H), 1.79-1.72 (m, 2H), 1.60-1.51 (m, 3H), 1.38-1.21 (m, 3H), 0.84 (dd, *J* = 11.4, 6.6 Hz, 6H). ^{13}C NMR (100 MHz, DMSO-d_6) δ 166.60, 159.24, 151.24, 149.89,

145.74, 134.61, 130.10, 130.06, 129.18, 129.02, 128.73, 119.06, 117.80, 115.57, 114.22, 111.11, 103.67, 79.30, 67.63, 58.05, 52.96, 48.34, 28.88, 26.13, 25.04, 23.80, 23.55, 22.04. HRMS (ESI): m/z calcd. For $C_{34}H_{43}BN_5O_4$ $[M+H]^+$: 596.3408, found: 596.3401.

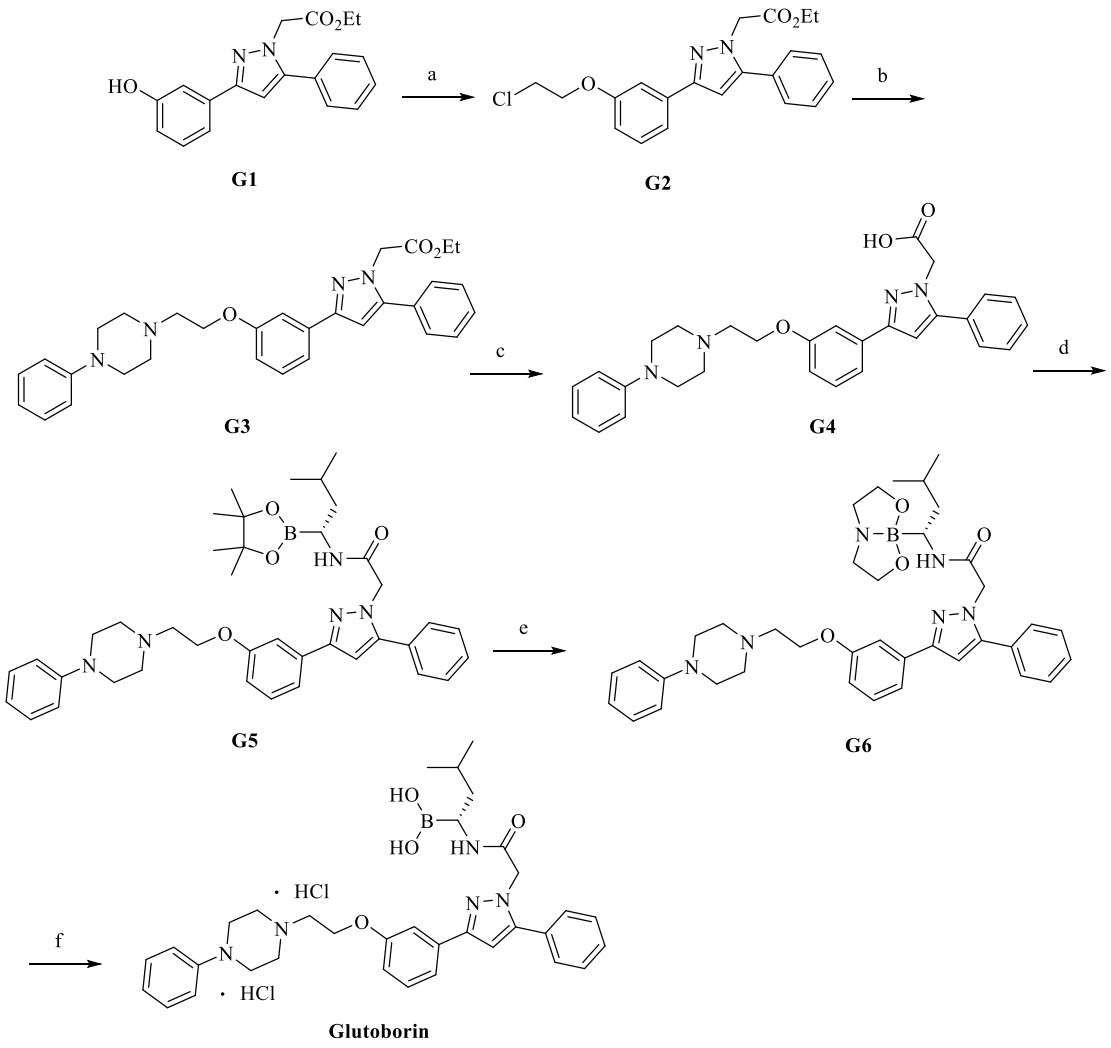

Scheme 1. **Synthesis of Glutoborin**. Reagents and conditions: (a) 2-chloroethyl 4-methylbenzenesulfonate, K_2CO_3, DMF/acetone, 80°C, 12 hrs, 90%. (b) i, NaI, acetone, reflux, 24 hrs, 99%; ii, 1-phenylpiperazine, K_2CO_3, DMF/acetone, 80°C, 12 hrs, 67%. (c) 4N hydrochloric acid, H_2O, reflux, overnight, 96%. (d) (*R*)-3-methyl-1-(4,4,5,5-tetramethyl-1,3,2-dioxaborolan-2-yl) butan-1-amine hydrochloride, HBTU, DIPEA, DMF, 0°C, 12 hrs, 64%. (e) diethanolamine, ether/ethyl acetate, 60%. (f) i, 4N hydrochloric acid, ethyl acetate/H_2O, ii, 2N hydrochloric acid in ethyl acetate, rt, overnight, 90%.

NMR spectrum of Glutoborin

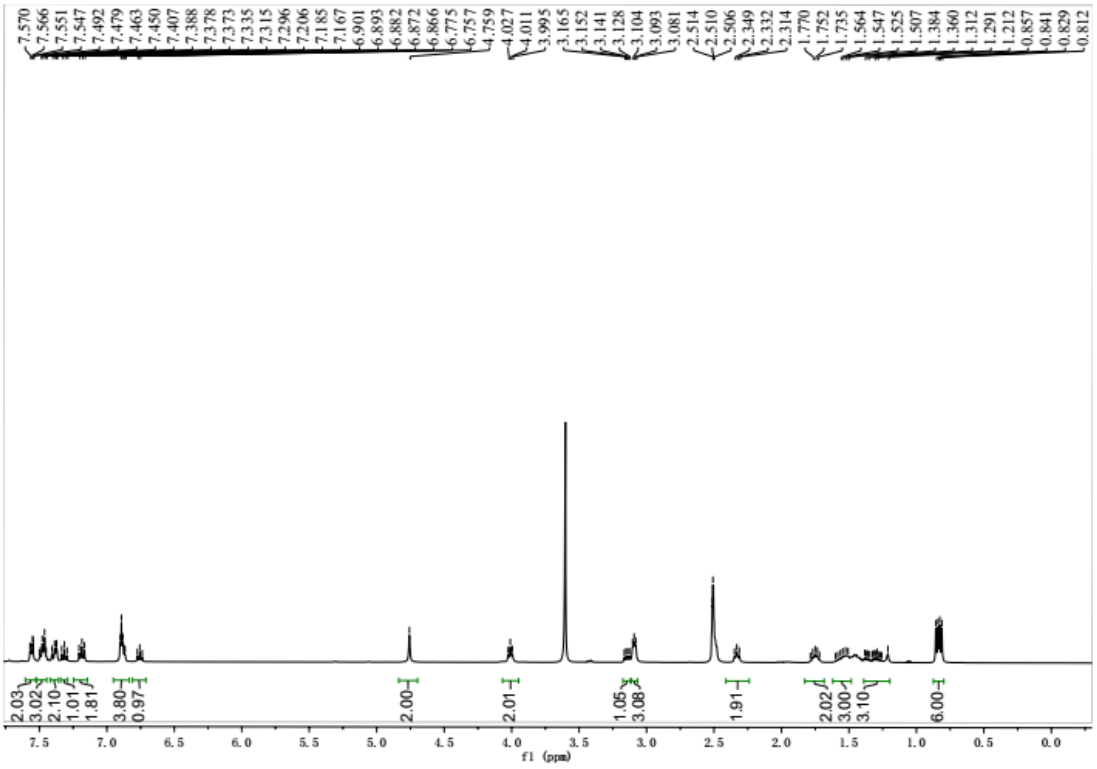

^{1}H NMR of Glutoborin (400 MHz, DMSO-d_6)

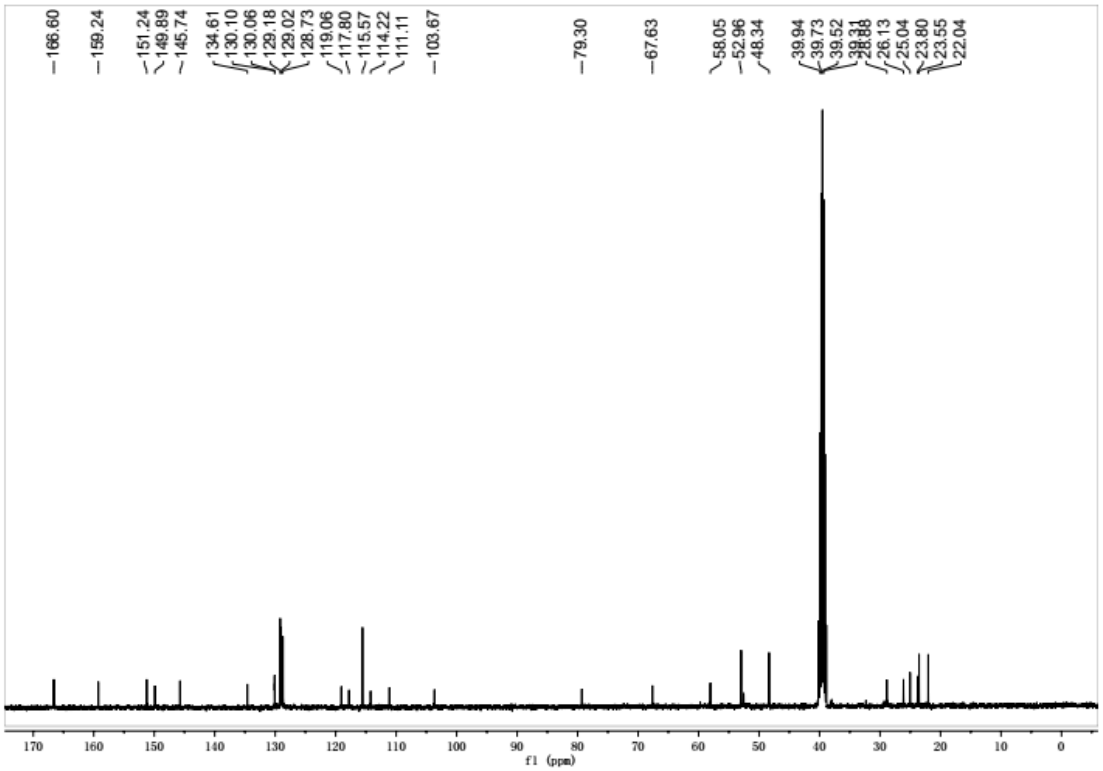

^{13}C NMR of Glutoborin (100 MHz, DMSO-d_6)

HRMS (ESI) spectrum of Glutoborin

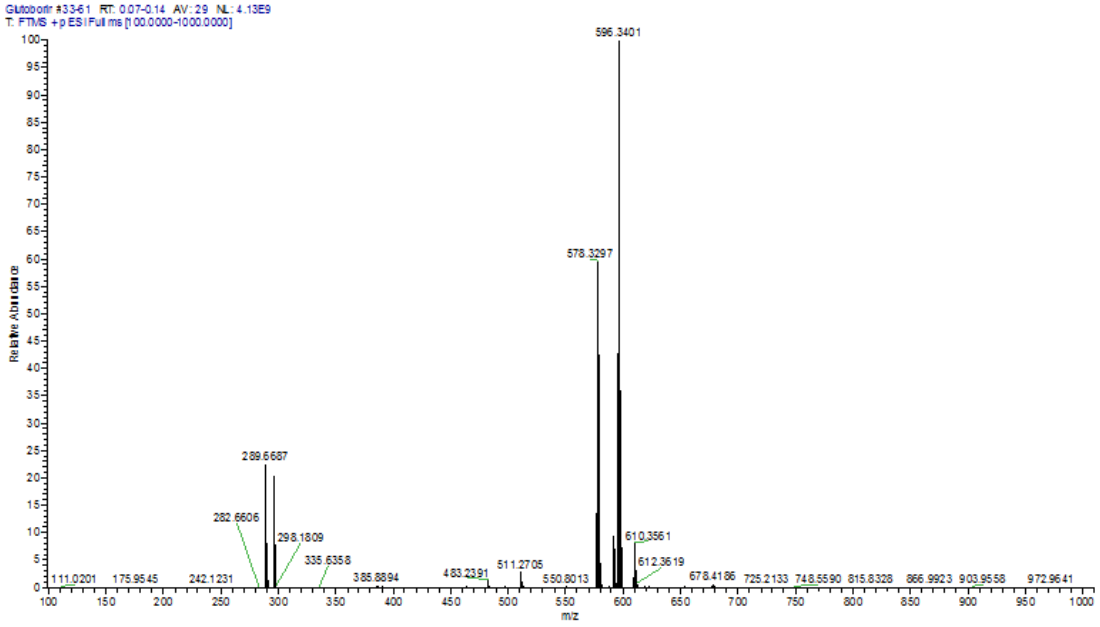

2. Supplementary Figures

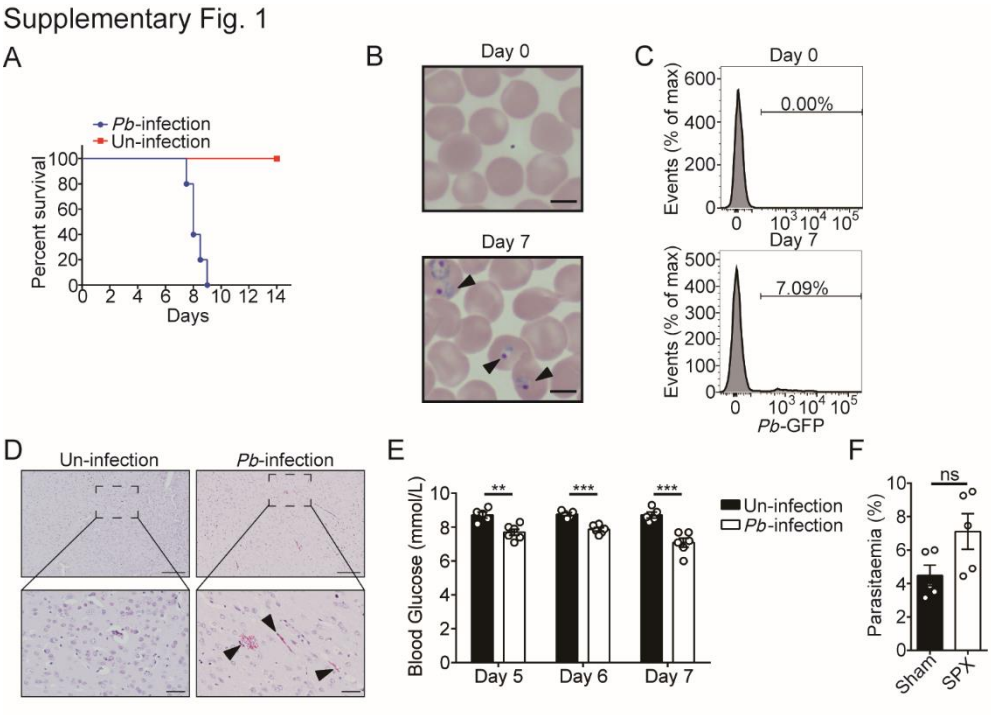

Supplementary Fig. 1 Construction and assessment of experimental CM (ECM) model. ECM model was established in mice via intraperitoneal injection of 1×10^4 iRBCs (**A-D**). **A** Survival curves of uninfected (Un-infection) and *Pb*-infected mice (*Pb*-infection) (n = 5 per group). **B** Giemsa staining of iRBCs from Un-infection and *Pb*-infection observed under a 100X oil-immersion lens (Day 7). Scale bar, 200 μm. **C** Representative flow cytometry bar plots illustrating the proportion of iRBCs in the blood based on GFP-expressing *Plasmodium*. **D** H&E staining of brain tissue from the Un-infection and *Pb*-infection. Black arrowheads indicate hemorrhagic spots or thrombi. Upper panel, scale bar, 250 μm. Lower panel, scale bar, 50 μm. **E** Blood glucose levels measured in serum collected from mice injected with 1×10^4 iRBCs on days 5, 6, and 7 post-infection (Un-infection, n = 5; *Pb*-infection, n = 6). **F** Proportion of iRBCs in the Sham and SPX groups on day 7 post-infection (n = 5 per group). Data are presented as mean ± SEM. Significance was determined using an unpaired Student's *t*-test. $^{**}P < 0.01$; $^{***}P < 0.001$; ns, $P > 0.05$.

Supplementary Fig. 2

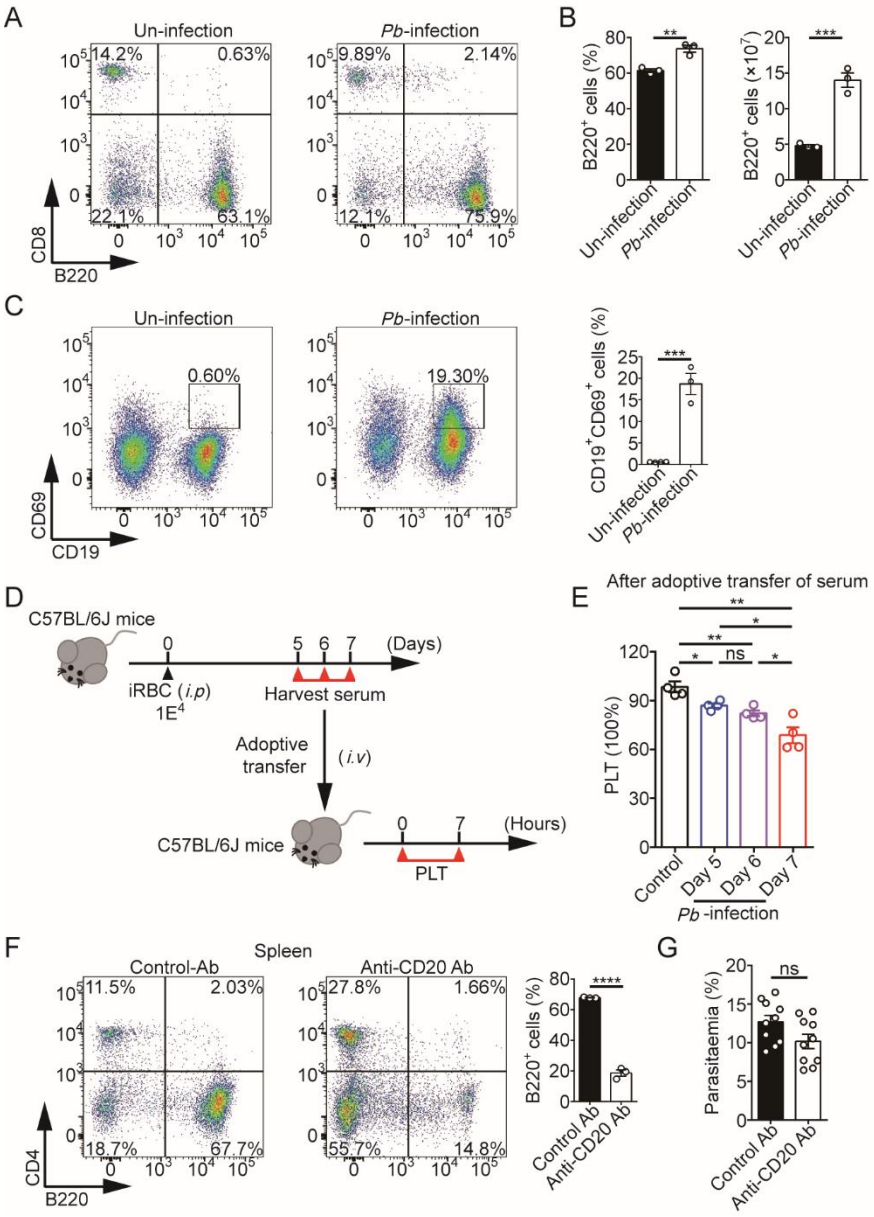

Supplementary Fig. 2 Splenic B cell expansion and anti-platelet antibody production in *Pb*-infected mice. A Representative flow cytometry plots of B200$^+$ cells in the spleens of Un-infection and *Pb*-infection on day 7 post-infection (n = 3 per group). **B** Bar plots showing the percentage (left) and absolute cell count (right) of B220$^+$ cells in the spleens of both groups. **C** Representative flow cytometry plots of CD19$^+$CD69$^+$ cells in the spleens of Un-infection (n = 4) and *Pb*-infection (n = 3) on day 5 post-infection. Right panel, bar plot showing the percentage of CD19$^+$CD69$^+$ cells in the spleens of both groups. To assess the presence of anti-platelet antibodies, mice were intraperitoneally injected with 1 × 10^4 iRBCs, and serum was collected on days 5, 6,

and 7 post-infection for adoptive transfer into uninfected recipient mice via tail vein injection. Platelet counts were measured 7 hrs after serum transfer (**D, E**). **D** Schematic representation of the adoptive transfer experiment. **E** Platelet counts in recipient mice after transfer of serum collected at different time points (n = 4 per group). **F** Representative flow cytometry plots of $B220^+$ cells in the spleen of Control Ab and Anti-CD20 Ab (Day5, n = 3 per group). Right panel, bar plot showing the percentage of $B220^+$ cells in the spleen of both groups. **G** As described in Fig. 2, proportion of iRBCs in mice treated with isotype control antibody (Control Ab) and anti-CD20 antibody (Anti-CD20 Ab) (n = 10 per group). Data are presented as mean ± SEM. Significance was determined using unpaired Student's *t*-test. $*P < 0.05$; $**P < 0.01$; $***P < 0.001$; $****P < 0.0001$; ns, $P > 0.05$.

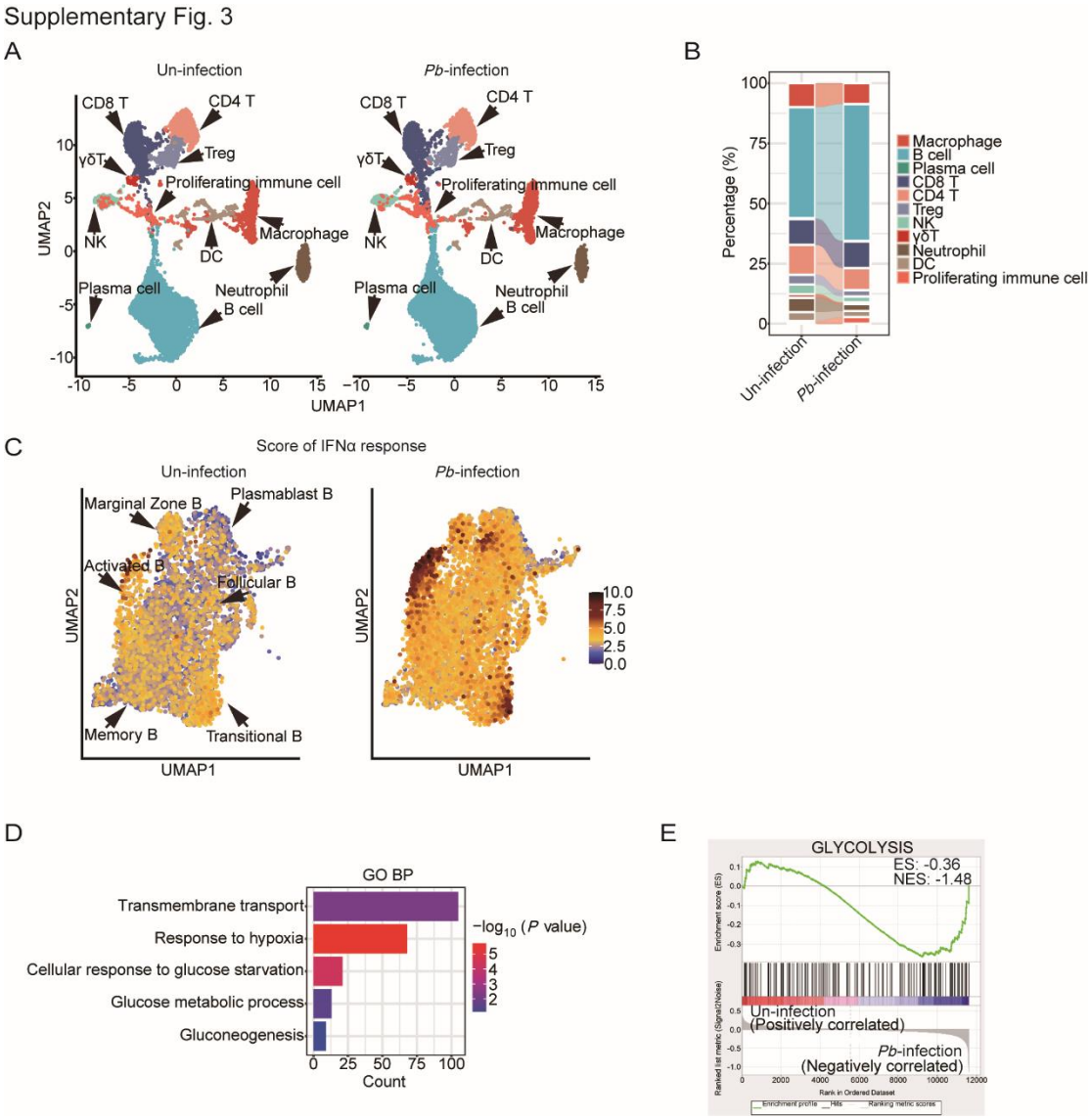

Supplementary Fig. 3 Single cell sequencing analysis of immune cell profiling in the spleens of *Pb*-infected mice. A As described in Fig. 3, UMAP visualization of eleven immune cell subsets in the spleen from Un-infection and *Pb*-infection. Cells were color-coded based on their assigned clusters. **B** Bar plot representing the proportion of each immune cell subset from Un-infection and *Pb*-infection. **C** Feature plot showing the IFN-α score of B cells from Un-infection and *Pb*-infection. **D** GO analysis showing pathway enrichment in activated MZMs from *Pb*-infection compared to Un-infection. **E** GSEA of comparing gene expression profiles in activated MZMs from the Un-infection and *Pb*-infection with the glycolysis gene set. ES, Enrichment Score; NES, Normalized Enrichment Score.

Supplementary Fig. 4

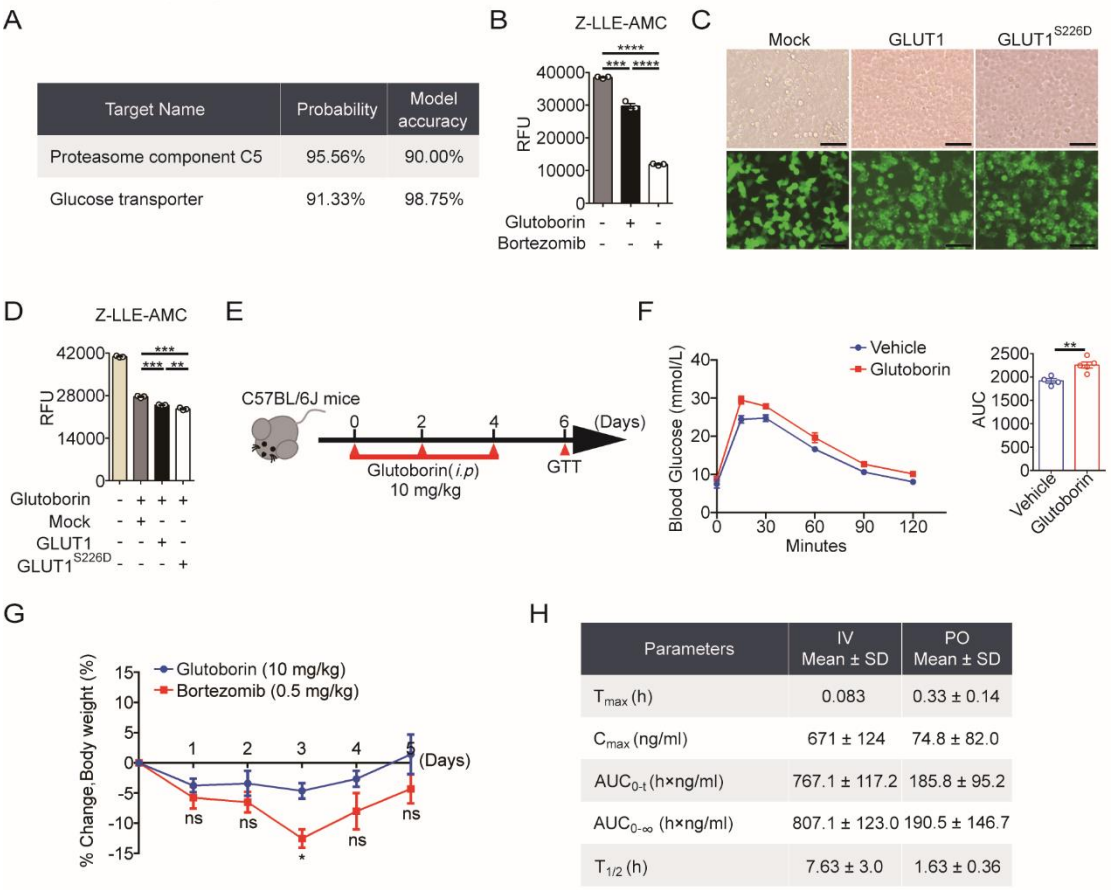

Supplementary Fig. 4 Glutoborin targets GLUT1 both *in vitro* and *in vivo*. **A** likelihood and accuracy of Glutoborin binding to proteasome and GLUT1 were predicted using the SwissTargetPrediction software. **B** As described in Fig. 4E, proteasome fluorescent substrate (Z-LLE-AMC, 50 μM) was added to the reaction system, followed by incubation at 37°C for 2 hrs. Fluorescence intensity was subsequently measured (Ex/Em = 350/450 nm). **C** Fluorescence microscopy analysis of HEK293T cells transfected with Mock-GFP, GLUT1-GFP, or GLUT1^{S226D}-GFP plasmids. Scale bar, 100 μm. **D** As described in Fig. 4G, proteasome fluorescent substrate (Z-LLE-AMC, 50 μM) was added to the reaction system, followed by incubation at 37°C for 3 hrs. Fluorescence intensity was subsequently measured (Ex/Em = 350/450 nm). Mice were administered vehicle or Glutoborin (10 mg/kg) via intraperitoneal injection on days 0, 2, and 4, followed by a 12-hour fasting period on Day 6. Blood glucose levels were then measured at 15, 30, 60, 90, and 120 minutes after glucose administration (**E, F**). **E** Schematic diagram of GTT. **F** Line graph of blood

glucose levels at different time points in two groups of mice. Right panel, statistical analysis of the area under the curve (AUC). **G** As described in Fig. 4I, line graph shows the changes in body weight over time in two groups of mice. **H** Average pharmacokinetic parameters of Glutoborin in plasma after a single intravenous injection (1 mg/kg) and oral administration (10 mg/kg) of Glutoborin in male SD rats. T_{max} (h): Time to peak; C_{max} (ng/ml): Peak concentration; $AUC_{0\text{-}t}$ (h×ng/ml): Area under the concentration-time curve from 0 to time t; $AUC_{0\text{-}\infty}$ (h×ng/ml): Area Under the Curve from 0 to infinity; $T_{1/2}$ (h): Elimination half-life. Data are presented as mean ± SEM. Significance was determined using unpaired Student's *t*-test. $*P < 0.05$; $**P < 0.01$; $***P < 0.001$; $****P < 0.0001$; ns, $P > 0.05$.

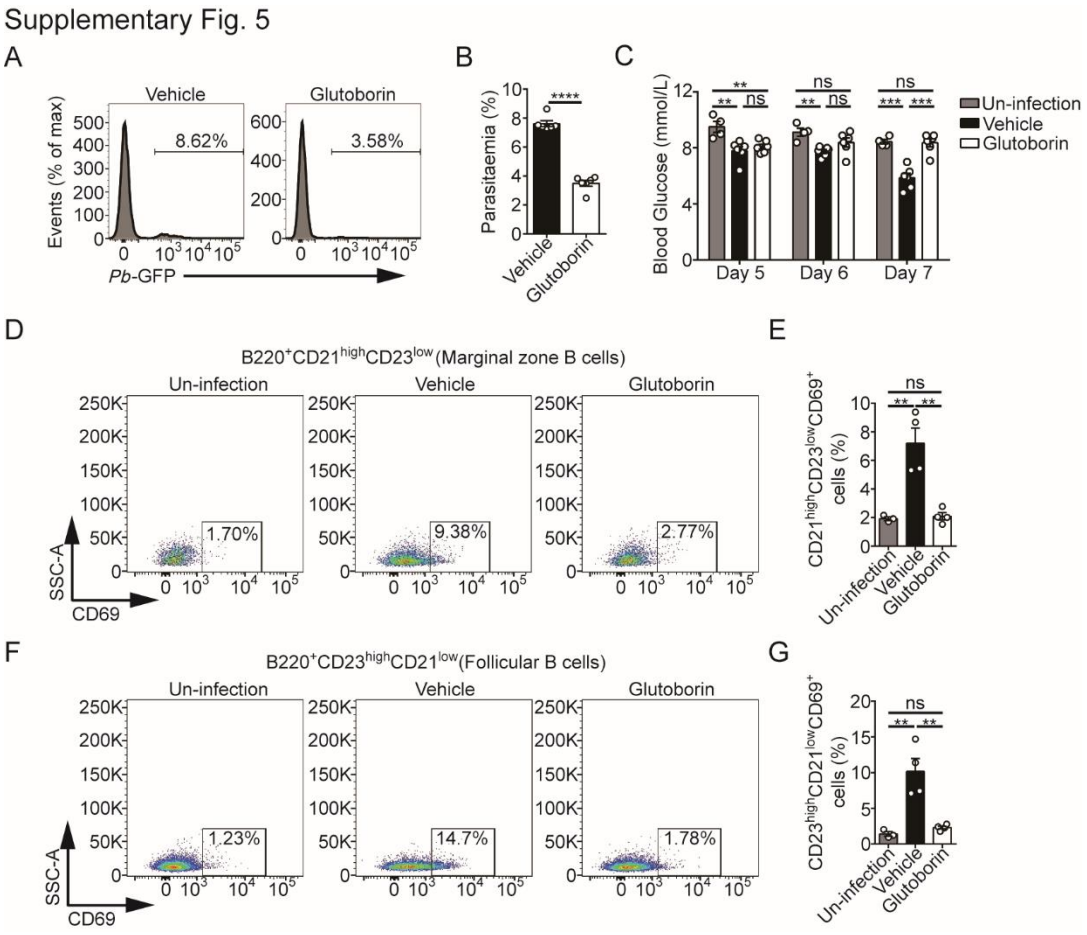

Supplementary Fig. 5 Glutoborin maintains blood glucose levels and inhibits B cell activation in *Pb*-infected mice. A Representative flow cytometry bar plots illustrate the proportion of iRBCs in blood of Vehicle- and Glutoborin-treated mice. **B**

Statistical analysis of the proportion of iRBCs in the blood of Vehicle- and Glutoborin-treated mice. (Day 7, n = 6 per group). **C** Statistical analysis of blood glucose levels in Un-infection, Vehicle- and Glutoborin-treated mice on day 5, 6, and 7 post-infection. **D** Representative flow cytometry plots illustrate CD69 expression on MZBs in the spleens of Un-infection (n = 3), Vehicle- (n = 4) and Glutoborin-treated mice (n = 4). **E** Bar plot shows the percentage of $CD69^+$ MZBs in the spleens of mice from different treatment groups. **F** Representative flow cytometry plots illustrate CD69 expression on FOBs in the spleens of Un-infection (n = 3), Vehicle- (n = 4) and Glutoborin-treated mice (n = 4). **G** Bar plot shows the percentage of $CD69^+$ FOBs in the spleens of mice from different treatment groups. Data are presented as mean ± SEM. Significance was determined using unpaired Student's *t*-test. $^{**}P < 0.01$; $^{***}P < 0.001$; $^{****}P < 0.0001$; ns, $P > 0.05$.

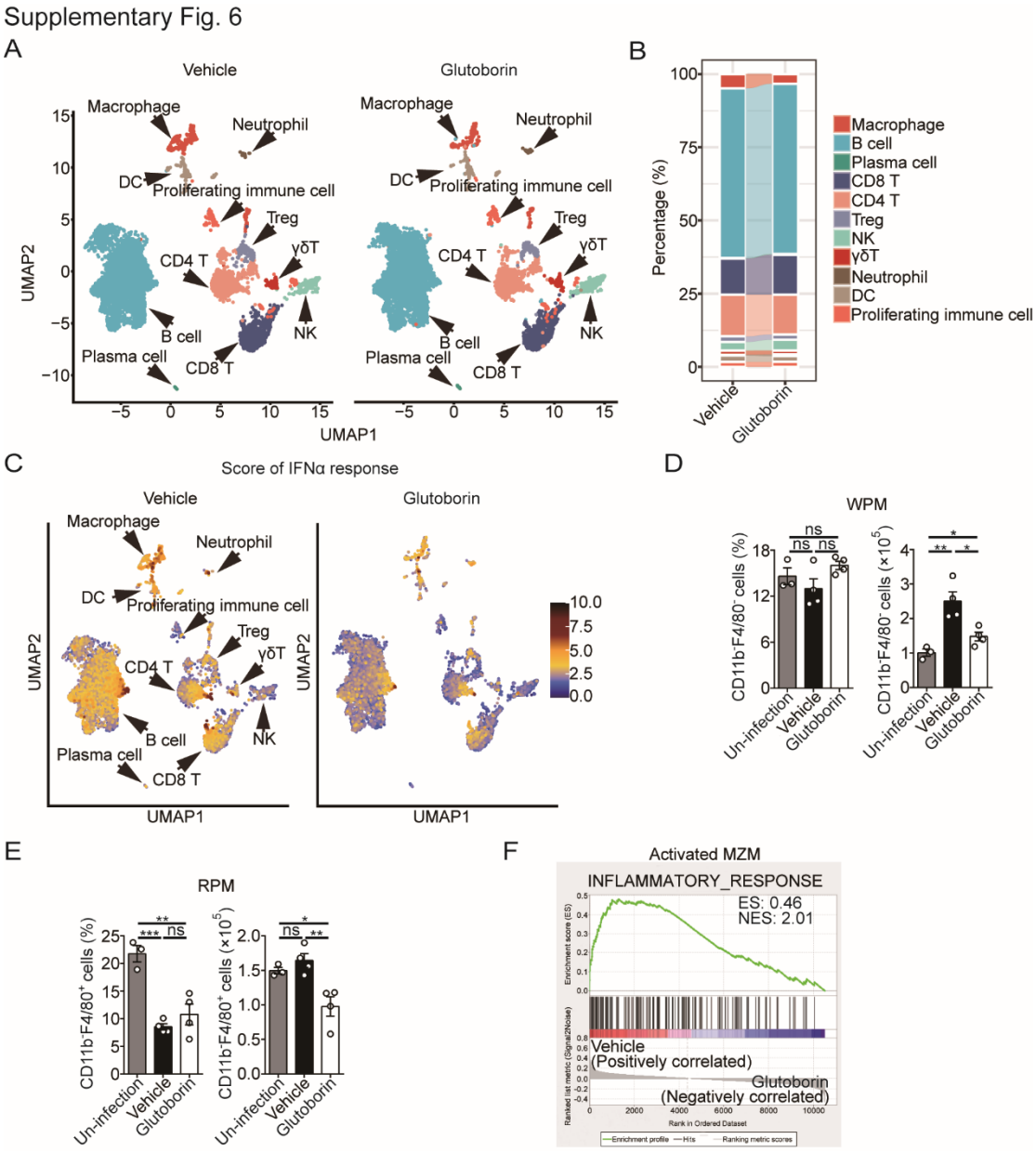

Supplementary Fig. 6 Glutoborin suppresses the inflammatory response in the spleens of *Pb*-infected mice. A UMAP visualization of eleven immune cell subsets in the spleen from Vehicle- and Glutoborin-treated mice. Cells were color-coded based on their assigned clusters. **B** Bar plot represents the proportion of each immune cell type in Vehicle- and Glutoborin-treated mice. **C** Feature plot shows the IFN-α score of immune cells in Vehicle- and Glutoborin-treated mice. **D, E** As described in Fig. 6C, bar plots show percentage (left) and absolute cell count (right) of WPM (**D**) and RPM (**E**) in the spleens of mice from different treatment groups. **F** GSEA of comparing gene profile in activated MZMs from the Vehicle- and Glutoborin-treated mice with inflammatory response gene set. ES, Enrichment Score; NES, Normalized Enrichment

Score. Data are presented as mean ± SEM. Significance was determined using unpaired Student's *t*-test. **P* < 0.05; ***P* < 0.01; ****P* < 0.001; ns, *P* > 0.05.

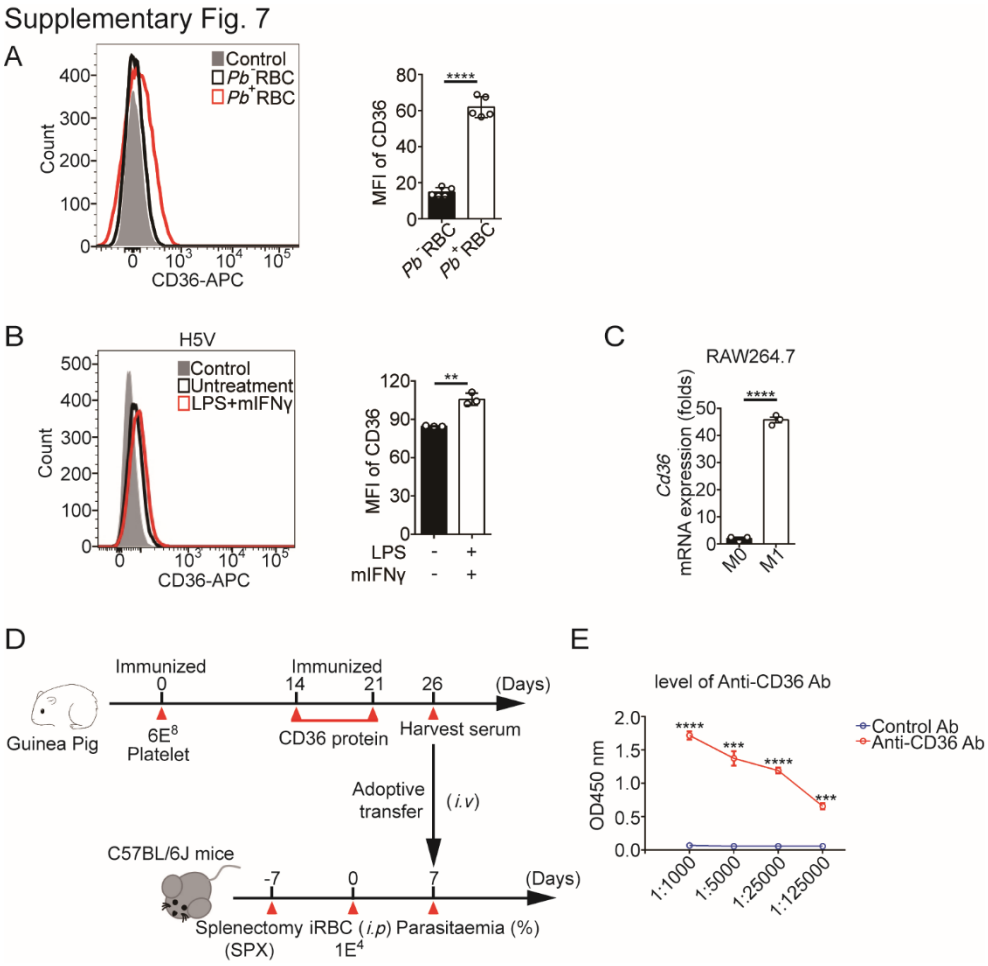

Supplementary Fig. 7 CD36 is expressed on iRBCs, endothelial cells and activated macrophages. A Representative flow cytometry bar plot illustrating the expression levels of CD36 on *Pb*$^{+}$ RBC and *Pb*$^{-}$ RBC. Right panel, mean fluorescence intensity (MFI) was used for statistical analysis. **B** Expression levels of CD36 were analyzed by flow cytometry in H5V cells treated with LPS (100 ng/ml) and mIFNγ (50 ng/ml) for 24 hrs. Right panel, MFI was used for statistical analysis. **C** Expression levels of *Cd36* were analyzed by qRT-PCR in RAW264.7 cells treated with (M1) or without (M0) LPS (50 ng/ml) for 12 hrs. **D** As described in Fig. 6, Schematic representation of the adoptive transfer of anti-CD36 antibodies. **E** The titer of anti-CD36 Abs was determined by ELISA. Data are presented as mean ± SEM. Significance was determined using unpaired Student's *t*-test. ***P* < 0.01; ****P* < 0.001; *****P* < 0.0001.

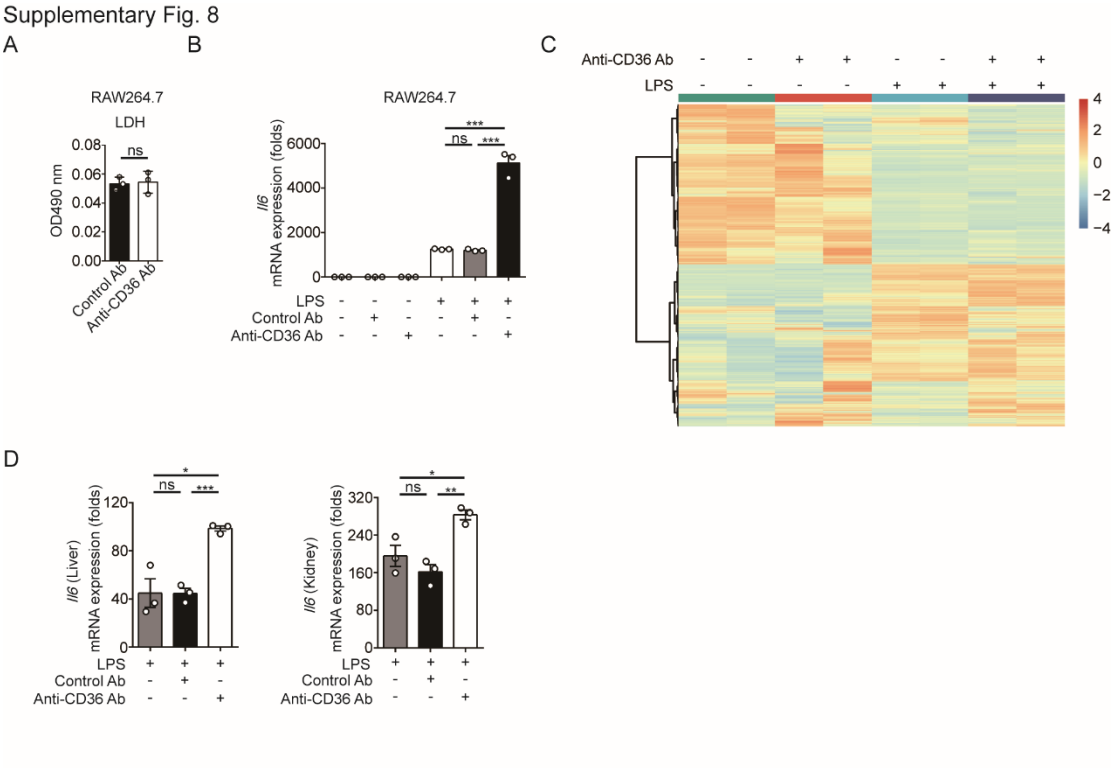

Supplementary Fig. 8 Supplementation of anti-CD36 Ab enhances LPS-induced inflammatory response. A LDH release assay of RAW264.7 cells treated with Control Ab or Anti-CD36 Ab (1:100 dilution), OD490 values were used for statistical analysis. **B** qRT-PCR analysis of expression levels of *Il6* in RAW264.7 cells treated with or without LPS, Control Ab and Anti-CD36 Ab. **C** Heatmap displaying different gene expression patterns across four groups. **D** qRT-PCR analysis of expression levels of *Il6* in the liver (left) and kidney (right) of mice treated with LPS (15 mg/kg), along with Control Ab (50 μl) or anti-CD36 Ab (50 μl) for 12 hrs (n = 3 per group). Data are presented as mean ± SEM. Significance was determined using unpaired Student's *t*-test. **P* < 0.05; ***P* < 0.01; ****P* < 0.001; ns, *P* > 0.05.

Supplementary Fig. 9

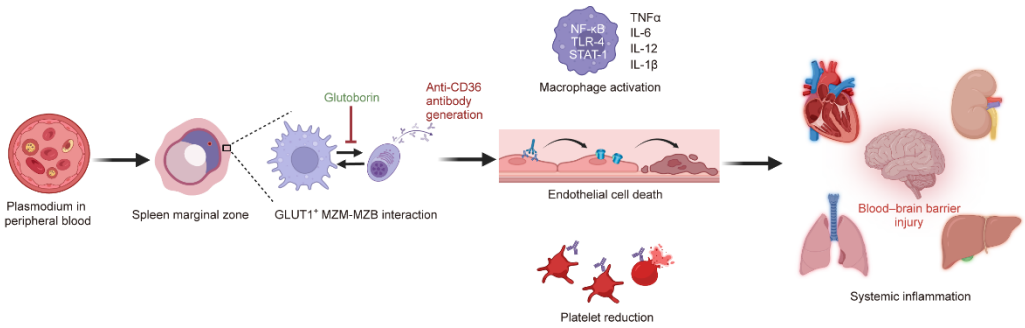

Cerebral malaria is an autoimmune-like disease

Supplementary Fig. 9 Pathological Mechanisms of Cerebral Malaria. In this model, *Plasmodium*-infected red blood cells are engulfed by GLUT1^{+} macrophages in the spleen marginal zone. These macrophages present antigens to marginal zone B cells, leading to B cell activation and the generation of anti-CD36 antibodies. These antibodies then mediate complement activation, causing damage to CD36^{+} platelets and endothelial cells. Additionally, anti-CD36 antibodies bind to CD36 on macrophages, enhancing macrophage activation via stimulating CD36-TLR4 axis, which further amplifies the inflammatory response. This dual action contributes to blood-brain barrier disruption and systemic inflammation, ultimately leading to lethal inflammatory damage.

3. Supplementary Tables

Supplementary Table 1

List of primers for qRT-PCR analysis in this study.

Gene name	Forward primer (5'->3')	Reverse primer (5'->3')
Actb	GGCTGTATTCCCCTCCATCG	CCAGTTGGTAACAATGCCATGT
Isg15	GGTGTCCGTGACTAACTCCAT	TGGAAAGGGTAAGACCGTCCT
Cxcl10	GACGGTCCGCTGCAACTG	GCTTCCCTATGGCCCTCATT
Tnf	GCCTCCCTCTCATCAGTTCTATG	CCACTTGGTGGTTTGCTACGA
Cd36	ATGGGCTGTGATCGGAACTG	TTTGCCACGTCATCTGGGTTT
Il1b	GCAACTGTTCCTGAACTCAACT	ATCTTTTGGGGTCCGTCAACT
Il6	TCTGCAAGAGACTTCCATCC	GAATTGCCATTGCACAACTC
Slc2a1	TCTGTCGGCCTCTTTGTTAATC	CCAGTTTGGAGAAGCCCATAA

Supplementary Table 2

List of marker genes of the clusters in scRNA-seq

cell_type	Marker_gene								
B	*Cd79a*	*Cd79b*	*Cd19*	*Ms4a1*	*Cr2*	-	-	-	-
Cd4T	*Cd247*	*Cd3e*	*Cd3d*	*Cd3g*	*Cd4*	-	-	-	-
Cd8T	*Cd247*	*CD3e*	*Cd3d*	*Cd3g*	*Cd8a*	*Cd8b1*	*Trac*	*Trbc1*	*Trbc2*
γδT	*Cd3e*	*Cd3d*	*Cd3g*	*Cd247*	*Tcrg-C2*	-	-	-	-
NK	*Gzmb*	*Klra3*	*Klrb1c*	*Klrk1*	*Ncr1*	*Prf1*	-	-	-
DC	*Sig;ech*	*Bst2*	*Cd83*	*Itgax*	*H2-Ab1*	*Xcr1*	*Clec9a*	*Itgam*	-
Macrophage	*Cd14*	*Adgre1*	*Cd68*	*Ly6c1*	*Csf3r*	*Itgam*	-	-	-
Neu	*Retnlg*	*Arg2*	*S100a8*	*Ceacam10*	*Fcgr3*	*Ncam1*	*Ly6g*	*Adgre1*	-
Plasma cell	*Tnfrsf17*	*Sdc1*	-	-	-	-	-	-	-
Treg	*Foxp3*	*Cd25*	*Cd247*	-	-	-	-	-	-
Proliferating immune cell	*Mki67*	*Top2a*	*Ptprc*	-	-	-	-	-	-

Source Data

Fig. 4F

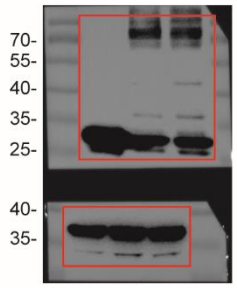

Fig. 7A

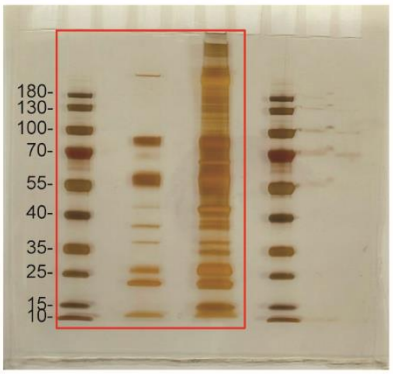

Fig. 7B

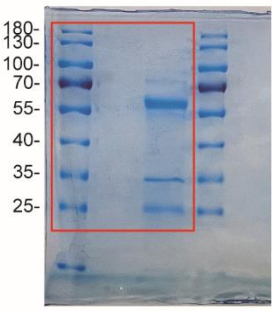

Fig. 8N

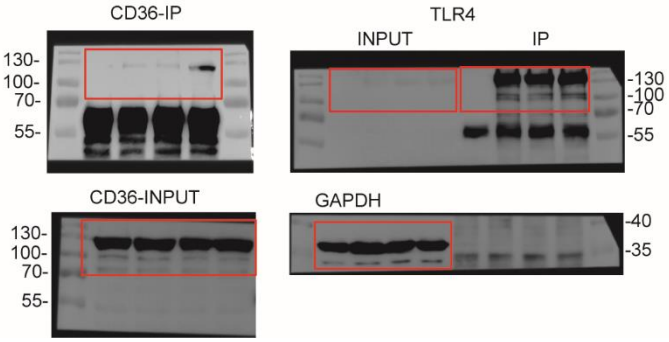

Title of manuscript:

Cerebral Malaria as an Autoimmune-like Disease Driven by Pathogenic B cell Responses and Systemic Inflammation

Authors:

Xin Sun[1*], Ridong Li[1*], Weixuan Wang[1], Wenyu Tian[1], Xin Zhang[1], Linjiang Han[1], Xuyang Zhao[1], Xiaoyan Xing[2], Yuhui Li[2], Runtao Li[3], Fuping You[1#] and Dan Lu[1#]

Submit to:

Cellular & Molecular Immunology

I assure that this manuscript has not been and will not be considered for print or electronic publication elsewhere other than as an abstract in any languages.
And all the authors agreed to submit this manuscript to Cellular & Molecular Immunology.
There is no conflict among the authors.

Signed by correspondence:

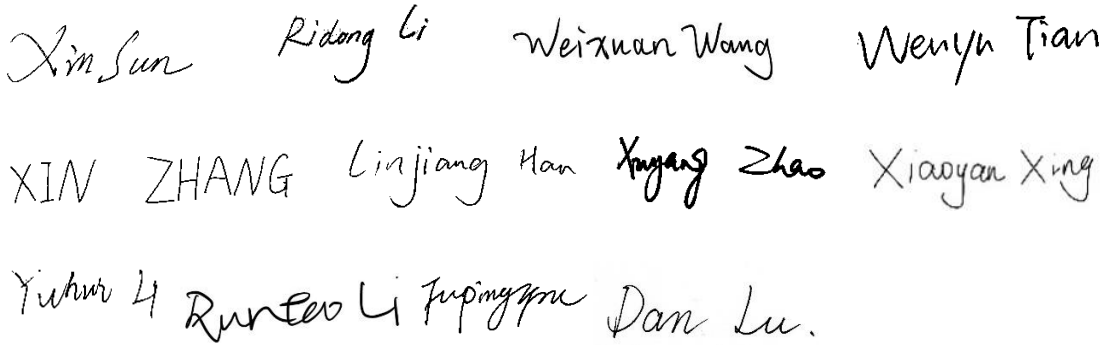

Date:2025/3/17

Affiliation:

[1]Institute of Systems Biomedicine, School of Basic Medical Sciences, NHC Key Laboratory of Medical Immunology, Beijing Key Laboratory of Tumor Systems Biology, Peking University, Beijing 100191, China.

[2]Department of Rheumatology and Immunology and Beijing Key Laboratory for Rheumatism and Immune Diagnosis (BZ0135), Peking University People's Hospital, Beijing 100044, China.
[3]State Key Laboratory of Natural and Biomimetic Drugs, School of Pharmaceutical Sciences, Peking University, Beijing 100191, China.

* These two authors contributed equally to this work.